

Inter-species molecular attraction effect in the development of a two-species mixing layer

Daniel T. Banuti *

California Institute of Technology, Pasadena, CA 91125, USA
The University of New Mexico, Albuquerque, NM 87131, USA

Josette Bellan † ‡

California Institute of Technology, Pasadena, CA 91125, USA
Jet Propulsion Laboratory, California Institute of Technology, Pasadena, CA 91109, USA

Simulations of fluid mixing occurring at high-pressures mandate the use of real-fluid equations of state to capture the effect of both intermolecular repulsive forces and attractive forces which are neglected in perfect gases. Dedicated mixing rules account for these forces by providing a generic mapping of the mixture state-space onto a pure fluid domain. However, the specific inter-species molecular forces depend on the particular characteristics of the molecular pairs under consideration, and typically require the knowledge of binary interaction coefficients $k_{\alpha\beta}$. The impact of $k_{\alpha\beta}$ on a flow field is as of now unclear; further, $k_{\alpha\beta}$ is unknown for many molecular pairs and when unknown, set to be null. This study addresses the impact of $k_{\alpha\beta}$ on the temporal evolution of a real-fluid mixing layer and uses Direct Numerical Simulation (DNS) to explore this impact. The results show differences between augmented attraction ($k_{\alpha\beta} < 0$) and diminished attraction ($k_{\alpha\beta} > 0$), affecting both fluid dynamics and diffusion processes. Specifically, in a binary mixing layer, it is observed that augmented attraction leads to delayed transition and mixing layer growth, manifested in the momentum layer thickness. The fractal dimension, which is a manifestation of interface corrugation, is calculated. These results provide an hitherto undocumented mechanism affecting the development of mixing layers.

I. Introduction

High-pressure injection and mixing processes occur in many technical combustion systems, such as gas turbines, Diesel engines, or rocket engines. In many cases, fluid thermodynamics can no longer be determined assuming perfect gas behavior, and the effect of intermolecular forces on thermodynamic and transport properties must be taken into account. Real gas equations of state (EOS), such as the Peng-Robinson EOS [1], include both repulsive and attractive forces that result in a representation of liquid, gaseous, and supercritical states [2]. The use of real fluid EOS is considered necessary for propulsion simulations [3, 4].

For cubic equations of state, such as the Peng-Robinson EOS, for pure fluids, only the knowledge of the critical pressure p_{cr} , the critical temperature T_{cr} , and the acentric factor ω are necessary; these values are usually tabulated. Mixtures are treated as virtual pure fluids, with the mixture parameters determined using mixing rules from the pure components. Several such mixing rules exist, and they are mostly heuristic in nature [5]. For the attractive term, mostly the geometric Bertholot mixing rule is utilized [2]. While mixing rules account for a general averaged interaction between the unlike molecular pairs, the physical reality is more complicated and depends on the exact molecules under consideration. To this end, a corrective factor, the binary interaction coefficient $k_{\alpha\beta}$, accounts for intermolecular forces deviating from the generalized average state [6].

However, $k_{\alpha\beta}$ is only available for a limited number of binary pairings, owing to the classical way of fitting it to experimental data for a specific mixture [5]. Values are typically tabulated [5, 7]. When $k_{\alpha\beta}$ is unknown, it is often assumed null. As of now, it is unclear whether neglecting $k_{\alpha\beta}$ in this manner has an impact on a flow field, both macroscopically (e.g. shear layer growth, fractal dimension) and microscopically (e.g. diffusion of heat and mass).

Thus, the purpose of this study is to compare the temporal evolution of two mixing layers of identical initial conditions – specifically identical density ratio, Mach number, and Reynolds number – but with different values of $k_{\alpha\beta}$,

* Assistant Professor, Department of Mechanical Engineering, UNM, AIAA Member. Formerly: Postdoctoral Scholar at Caltech.

† Senior Research Scientist, AIAA Fellow

‡ Corresponding author: josette.bellan@jpl.nasa.gov

accounting for augmented and diminished strengths of the intermolecular attractive forces, respectively.

II. Governing equations

A. Differential conservation equations

The conservation equations for mass, momentum, total energy e_t and species partial mass are:

$$\frac{\partial \rho}{\partial t} + \frac{\partial}{\partial x_j} [\rho u_j] = 0, \quad (1)$$

$$\frac{\partial}{\partial t} (\rho u_i) + \frac{\partial}{\partial x_j} [\rho u_i u_j + p \delta_{ij} - \sigma_{ij}] = 0, \quad (2)$$

$$\frac{\partial}{\partial t} (\rho e_t) + \frac{\partial}{\partial x_j} [(\rho e_t + p) u_j - u_i \sigma_{ij} + q_j] = 0, \quad (3)$$

$$\frac{\partial}{\partial t} (\rho Y_\alpha) + \frac{\partial}{\partial x_j} [\rho Y_\alpha u_j + J_{\alpha j}] = 0, \quad (4)$$

where $\alpha \in [1, N - 1]$, t represents the time, x is a Cartesian coordinate, subscripts i and j refer to the spatial coordinates, ρ is the mass density, u_i is the velocity, $e_t = e + u_i u_i / 2$, e is the internal energy, Y_α is the mass fraction of species α and N is the number of species, σ_{ij} is the Newtonian viscous stress tensor

$$\sigma_{ij} = \mu \left(2S_{ij} - \frac{2}{3} S_{kk} \delta_{ij} \right), \quad S_{ij} = \frac{1}{2} \left(\frac{\partial u_i}{\partial x_j} + \frac{\partial u_j}{\partial x_i} \right), \quad (5)$$

where μ is the viscosity, S_{ij} is the strain-rate tensor, and $J_{\alpha j}$ and q_j are the j -direction species- α mass flux and heat flux, respectively.

The conservation equations have been presented in extensive details in [8] and [9]. These conservation equations are based on fluctuation-dissipation theory [10] which uses the complete form of the species-diffusion fluxes and of the heat flux, all of which utilize the full matrices of mass-diffusion coefficients and thermal-diffusion factors derived by [11]. The equations are solved in conservative form.

B. Equation of state

The system of conservation equations is complemented by the Peng-Robinson (PR) [1] EOS

$$p = \frac{R_u T}{(v_{PR} - b_{\text{mix}})} - \frac{a_{\text{mix}}}{(v_{PR}^2 + 2b_{\text{mix}} v_{PR} - b_{\text{mix}}^2)}. \quad (6)$$

Here, R_u is the universal gas constant, v_{PR} is the molar PR volume, and $v = v_{PR} + v_s$ where v_s is a volume correction to make the PR EOS more accurate; a_{mix} and b_{mix} are functions of the temperature T and species- α mole fraction X_α

$$a_{\text{mix}} = \sum_{\alpha=1}^N \sum_{\beta=1}^N X_\alpha X_\beta \sqrt{a_\alpha a_\beta} (1 - k_{\alpha\beta}); \quad b_{\text{mix}} = \sum_{\alpha=1}^N X_\alpha b_\alpha \quad (7)$$

where the computation of a_α , a_β and b_α is described in detail elsewhere [8]. Reference data for the relevant species are calculated using the highly accurate Lee-Kesler method [5, 12] based on an improved Benedict-Webb-Rubin type EOS, as determined before for the species used herein [13].

III. Binary interaction coefficients

The binary interaction coefficient $k_{\alpha\beta}$ in Eq. (7) is a corrective factor that increases accuracy of the EOS mixing rules to account for the actual molecular interaction. Its impact on mixture behavior is substantial; bubble and vapor curves cannot be reproduced quantitatively, and even the general mixture Type according to the van Konynenburg-Scott classification [14] cannot be determined without an appropriate value. The difficulty lies in the fact that $k_{\alpha\beta}$ cannot be

determined from first principles, but it is instead typically found by fitting vapor-liquid-equilibrium (VLE) calculations to experimental data [2].

An alternative was proposed by Jaubert and his group [15–17]. The authors do not fit $k_{\alpha\beta}$ for each binary molecular pair, but instead decompose each molecule into groups (such as CH₃, CH₂, etc.) to evaluate the contribution of these groups to $k_{\alpha\beta}$ as building blocks. Then, $k_{\alpha\beta}$ is expressed as a function of T , species-specific critical parameters, and the relevant groups. Notably, $k_{\alpha\beta}$ is not a function of p . A regression analysis is performed over a database containing many species according to their respective group composition, rather than a binary pair. Then, knowledge of the groups is the only information necessary to evaluate $k_{\alpha\beta}$, even for species without VLE measurements. For example, fitted coefficients for the groups CH₃ and CH₂ allow to determine $k_{\alpha\beta}$ for interactions between all pairs of alkanes. In this way, the Peng-Robinson $k_{\alpha\beta}$ can be determined for new species, as long as data are available for the constitutive groups of that species. The approach is reminiscent of Benson’s group additivity theory [18] and of the method of Kourdis and Bellan [19] for developing reduced kinetics.

The set of tabulated (tab) and computed interaction coefficients using group contribution (gc) method will be referred to as $k_{\alpha\beta}^{\text{tab}}$ and $k_{\alpha\beta}^{\text{gc}}$, and is listed in Table 1. The $k_{\alpha\beta}^{\text{gc}}$ from the group contribution method are averaged over the temperature in the simulation $T = \{600, 1000\}$ K and used as constant values in the simulation; general theory states that the $k_{\alpha\beta}$ T -dependence is small [5].

α	β	$k_{\alpha\beta}^{\text{tab}}$ [7]	$k_{\alpha\beta}^{\text{gc}}$ [20]
<i>n</i> -C ₇ H ₁₆	N ₂	0.1441	-0.2156

Table 1 Binary interaction coefficients.

IV. Configuration and initial conditions

The configuration is that of a temporal mixing layer having two streams, each stream initially hosting a single species: C₇H₁₄ (denser fluid) in the lower stream and N₂ (lighter fluid) in the upper stream. Initially, the layer hosts four spanwise vortices and the mean flow is initially perturbed, thereby triggering vortex growth and merging, as well as species mixing. The layer evolves through two vortex pairings, a process from which ultimately a single vortex emerges in which small scales proliferate.

Two cases are here compared in order to assess the effect of two values of the binary interaction coefficients, $k_{\alpha\beta}^{\text{tab}}$ and $k_{\alpha\beta}^{\text{gc}}$, on the evolution of the layer and the compositional field. The test DNS realizations are all at $p = 60$ bar with an initial Reynolds number $\text{Re}_0 = 1000$ (see [9] for the definition). The grid size is $480 \times 530 \times 288$, having been shown to resolve all scales relevant to dissipation [13]. The initial conditions are listed in Table 2. The current state of knowledge is such that, the expectation is that, having an identical density ratio, Mach number and momentum flux ratio, these layers will develop identically.

V. Results

The exposition of the results starts with integral values, then proceeds with the fuel mole fraction fields, the fractal dimension of the mixing layer, and finally addresses the density gradient.

A. Integral values

Figure 1 illustrates the temporal evolution of the momentum layer thickness, δ_m . A non-dimensional time is defined, $t^* = t\Delta U_0/\delta_{\omega,0}$, where ΔU_0 is the initial velocity difference between streams and $\delta_{\omega,0}$ is the initial vorticity thickness computed from the initial mean velocity (see [9] for the details). The results show that despite identical initial conditions, the shear layers using tabulated values of $k_{\alpha\beta}^{\text{tab}}$ and $k_{\alpha\beta}^{\text{gc}}$ develop differently. The momentum layer thickness (see [9] for the definition) growth is initially slower for $k_{\alpha\beta}^{\text{gc}}$, but eventually reaches higher growth rates. A local plateau eventually establishes at $t^* \approx 100$, signifying the merging of a two-vortex structure to a single vortex, and the $\delta_m/\delta_{\omega,0}$ value at this plateau reaches a larger magnitude for $k_{\alpha\beta}^{\text{gc}}$.

T_U	K	1000
T_L	K	600
ρ_U	kg/m ³	20.06
ρ_L	kg/m ³	260.09
ρ_L/ρ_U	-	12.97
$(\rho u)_U$	kg/m ² s	5141.98
$(\rho u)_L$	kg/m ² s	18515.44
$(\rho u)_L/(\rho u)_U$	-	3.60
Z_U	-	1.02
Z_L	-	0.47

Table 2 Flow initial conditions. Subscripts U and L denote the upper and lower layer, respectively.

Fig. 1(b) shows the t^* evolution of the magnitude of the spanwise positive vorticity (see [9] for the definition). The development of the (gc) case is delayed compared to (tab), although the same magnitude is reached at a later t^* value.

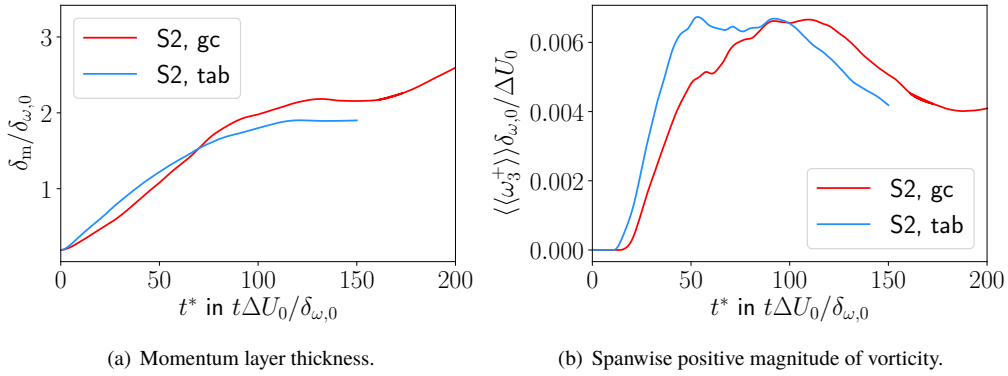


Fig. 1 Evolution of integral shear layer quantities as a function of t^* .

B. Fuel mole fraction field

An understanding of the developing composition field can be gained from Figs. 2 and 3, showing a comparison of the temporal evolution of the fuel mole fraction for the two values of the binary interaction coefficient. At $t^* \approx 40$, the four-vortex structure has become a two-vortex structure, which merge to a single vortex at $t^* \approx 100$.

Consistent with Fig. 1, the layer computed using $k_{\alpha\beta}^{gc}$ appears to have delayed species-mixing development and the composition field exhibits a decreased number of smaller structures. At $t^* \approx 40$ in Fig. 2, N_2 is seen to be entrained into C_7H_{16} for the simulation using $k_{\alpha\beta}^{tab}$, whereas the simulation using $k_{\alpha\beta}^{gc}$ exhibits a stricter separation of species distributions. This also indicates that the fuel-side boundary between the mixing layer and the fuel stream is more convoluted for $k_{\alpha\beta}^{tab}$ than for $k_{\alpha\beta}^{gc}$. At $t^* > 80$, however, the fuel-side boundary appears similarly convoluted for both cases. Generally, the nitrogen-side boundary appears smoother than the fuel-side boundary. The apparently lesser convoluted structures observed initially for $k_{\alpha\beta}^{gc}$ suggest delayed mixing and perhaps a reduced density gradient.

C. Fractal dimension of the mixing layer

In order to measure interfacial roughness accurately, we determine the fractal dimension D_f of the shear layer interface. Specifically, we analyze the fractal dimension for interfaces defined by a given fuel mole fraction z . As a preliminary to computing D_f , in Fig. 4 regions of $z = 0.001, 0.25, 0.5, 0.75$ for the (tab) simulation, going from regions

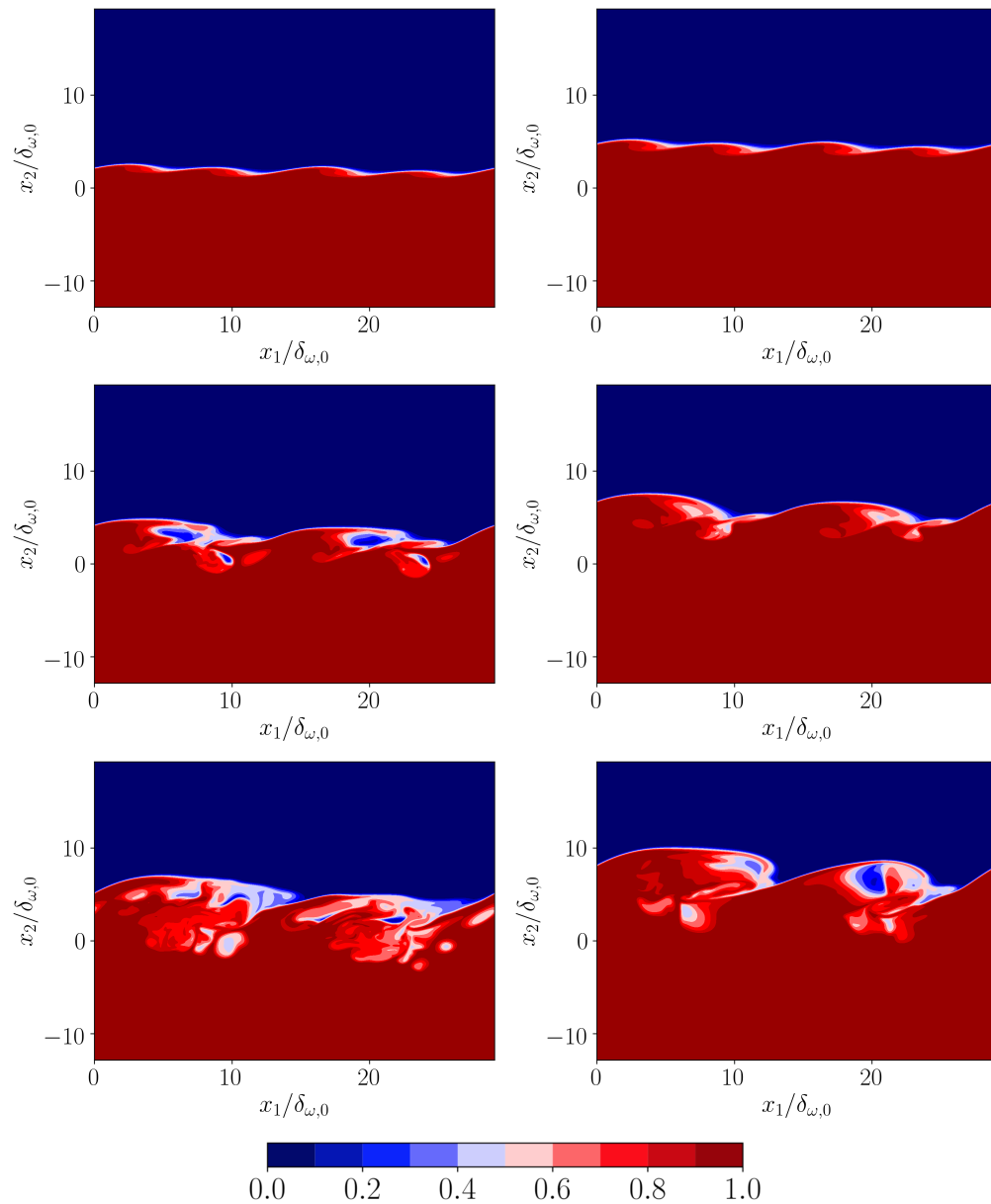


Fig. 2 Distribution of fuel mole fraction z for (tab) - left column, and (gc) - right columns, for $t^* = [20, 40, 60]$ from top to bottom. Shown is the $x_3/L_3 = 1/16$ plane, where $\delta_{\omega,0}$ is the initial vorticity thickness of the layer.

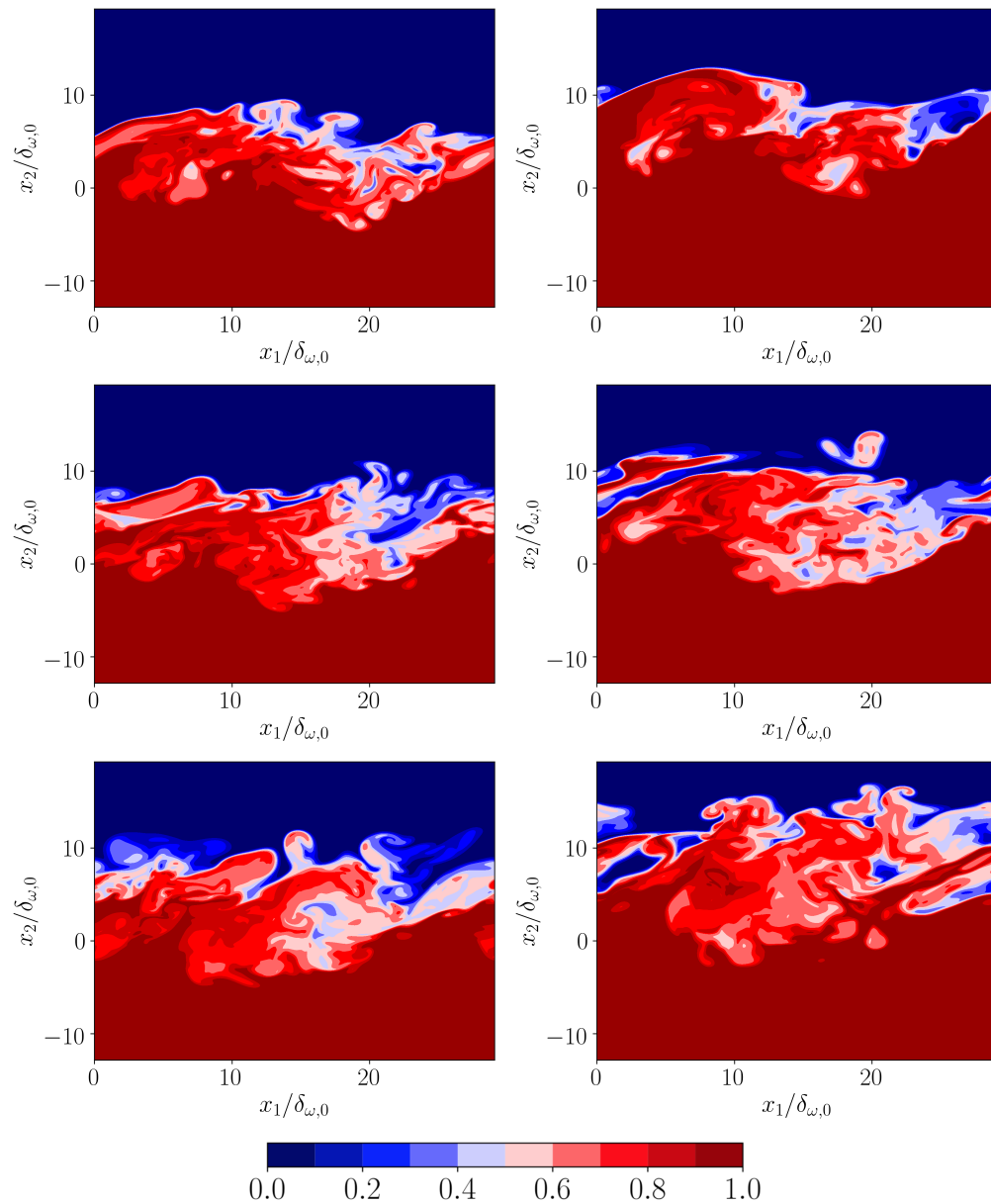


Fig. 3 Distribution of fuel mole fraction z for (tab) - left column, and (gc) - right columns, for $t^* = [80, 100, 120]$ from top to bottom. Shown is the $x_3/L_3 = 1/16$ plane, where $\delta_{\omega,0}$ is the initial vorticity thickness of the layer.

where only very small amount of the denser fluid exist to regions essentially dominated by the denser fluid. Only the mixing layer is represented, and the regions of pure fluid do not appear. It is clear that the interfaces between regions of constant z becomes more convoluted as t^* increases, and the lighter-fluid side appears smoother than the denser fluid side. For $z \rightarrow 0$ or $z \rightarrow 1$ the contour is smooth, with the expectation that $D_f \rightarrow 1$.

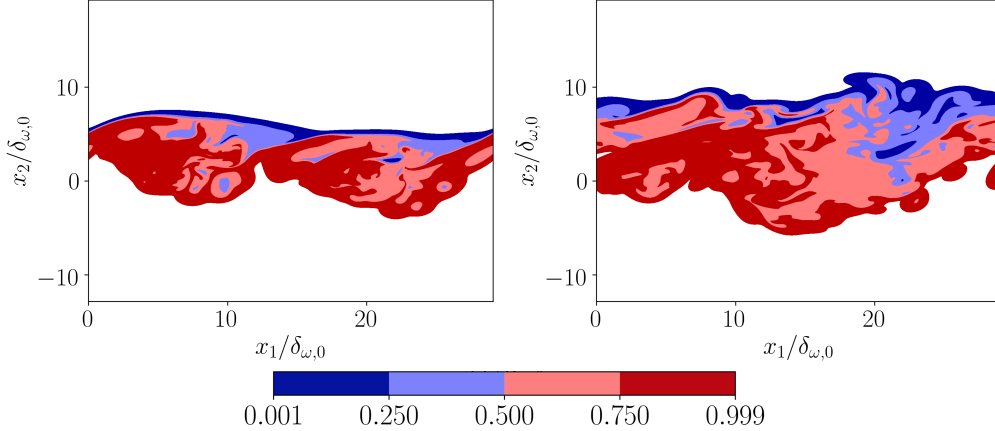


Fig. 4 Regions of $z = 0.001, 0.25, 0.5, 0.75$ and 0.999 for (tab) at $t^* = 60$ (left) and $t^* = 100$ (right).

In figure 5 (tab) and (gc) results are compared at increasing t^* values, and the information is consistent with that of Fig. 4. Each point $D_f(z)$ corresponds to the fractal dimension of the z iso-contour defining a constant z region. Indeed, $D_f \approx 1$ for early times and towards the pure fluid boundaries. Consistent with Figs. 2 and 3, the fuel side ($z \rightarrow 1$) is deforms first until $t^* = 100$ the mixing layer has deformed over the entire composition range. Notably, (tab) reaches higher values of D_f earlier, and the deformation affects regions of small z earlier during the layer evolution. After $t^* = 100$, the D_f distributions of both cases are comparable.

D. Density gradient

Figures 6 and 7 show that $|\nabla\rho|$ is representative of the changes between iso-contours of $z = \text{constant}$ regions (see Figs. 2, 3 and 4). The results show that, consistent with the larger diversity of states obtained, using $k_{\alpha\beta}^{gc}$ increases the resulting $|\nabla\rho|_{\max}$ compared to $k_{\alpha\beta}^{\text{tab}}$. This finding indicated that using $k_{\alpha\beta}^{gc}$ results in reduced mixing and accordingly foreseen increased scalar dissipation.

Visualizations of the density gradient field in Figs. 6 and 7 support the notion of a different diffusional evolution of the mixing layer for the (tab) and (gc) cases. Initially, the (tab) $|\nabla\rho|$ field seems more diffusive, by $t^* = 60$ it is clear that its boundaries appear more wrinkled for (tab), and by $t^* = 80$ small round structures are formed on the nitrogen side of (tab). Similarly, high $|\nabla\rho|$ separate round structures appear into the fuel stream for (tab) at $t^* = 100$ and for (gc) at $t^* = 120$. To quantitatively evaluate $|\nabla\rho|$, its probability density function is evaluated for the (tab) and (gc) at different t^* values and is displayed in Fig. 8. Figure 8 indicates that (tab) and (gc) case develop qualitatively similarly, but that quantitative differences exist, particularly in the high $|\nabla\rho|$ -value regions.

VI. Conclusions

The study evaluates the impact of the binary interaction coefficient $k_{\alpha\beta}$, a corrective factor accounting for inter-species attractive forces, on the development of a two species turbulent shear layer under real fluid conditions. Two mixing layers of identical initial conditions have been simulated using Direct Numerical Simulation; the only difference between simulations is the value of $k_{\alpha\beta}$. The results show that the qualitative evolution of the mixing layers is similar, but the quantitative evolution is different both from the fluid dynamic (entrainment) and compositional viewpoint (species diffusion). Specifically, it was found that a $k_{\alpha\beta} < 0$, signifying augmented inter-species attraction, results in a delayed development of momentum layer thickness. These results underline the importance of the accurate value of $k_{\alpha\beta}$. Further, the results also call to caution, as both values of $k_{\alpha\beta}$ are taken from published literature for the mixture and further studies are necessary to determine which value is accurate.

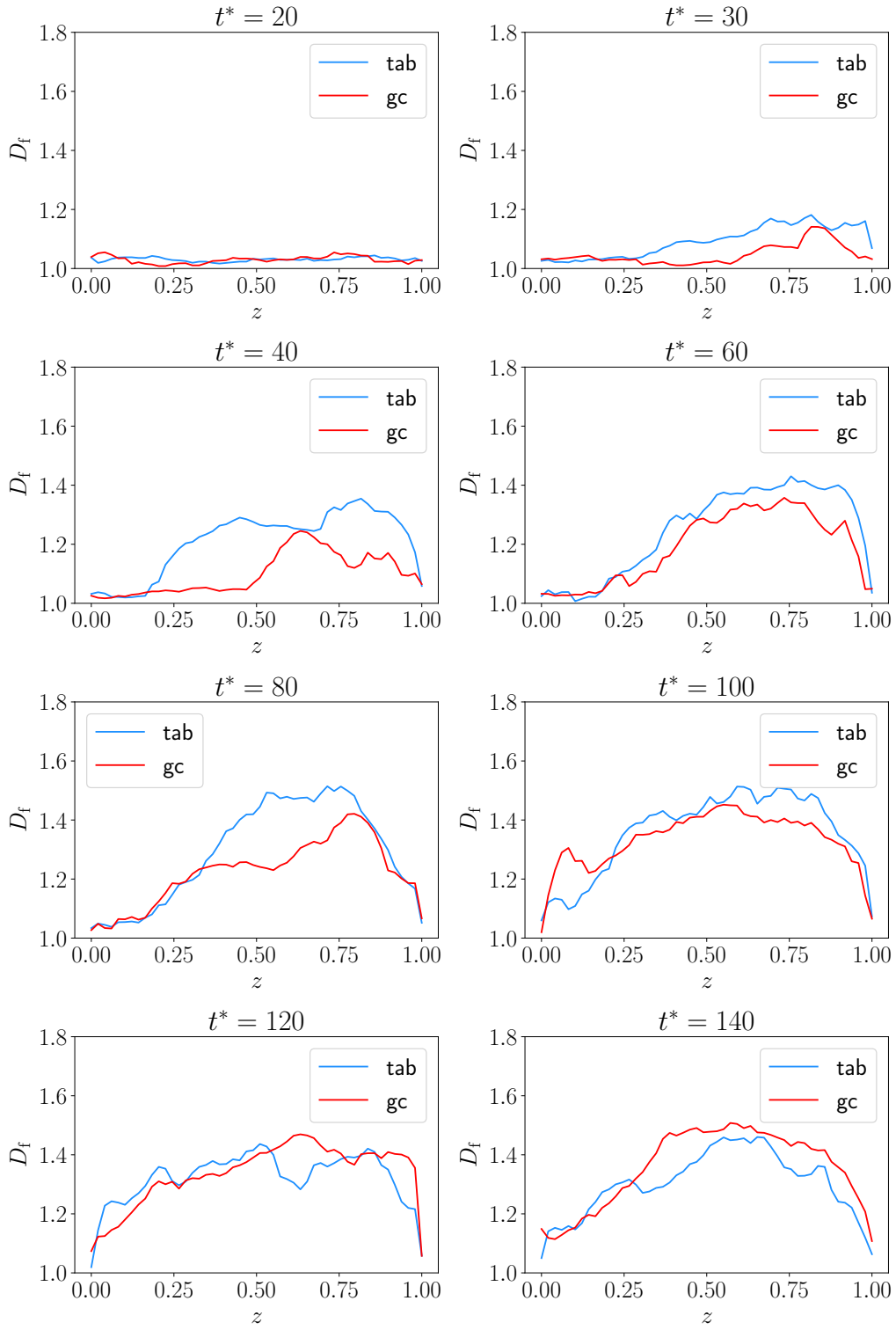


Fig. 5 Evolution of the fractal dimension D_f as a function of z for various values of t^* .

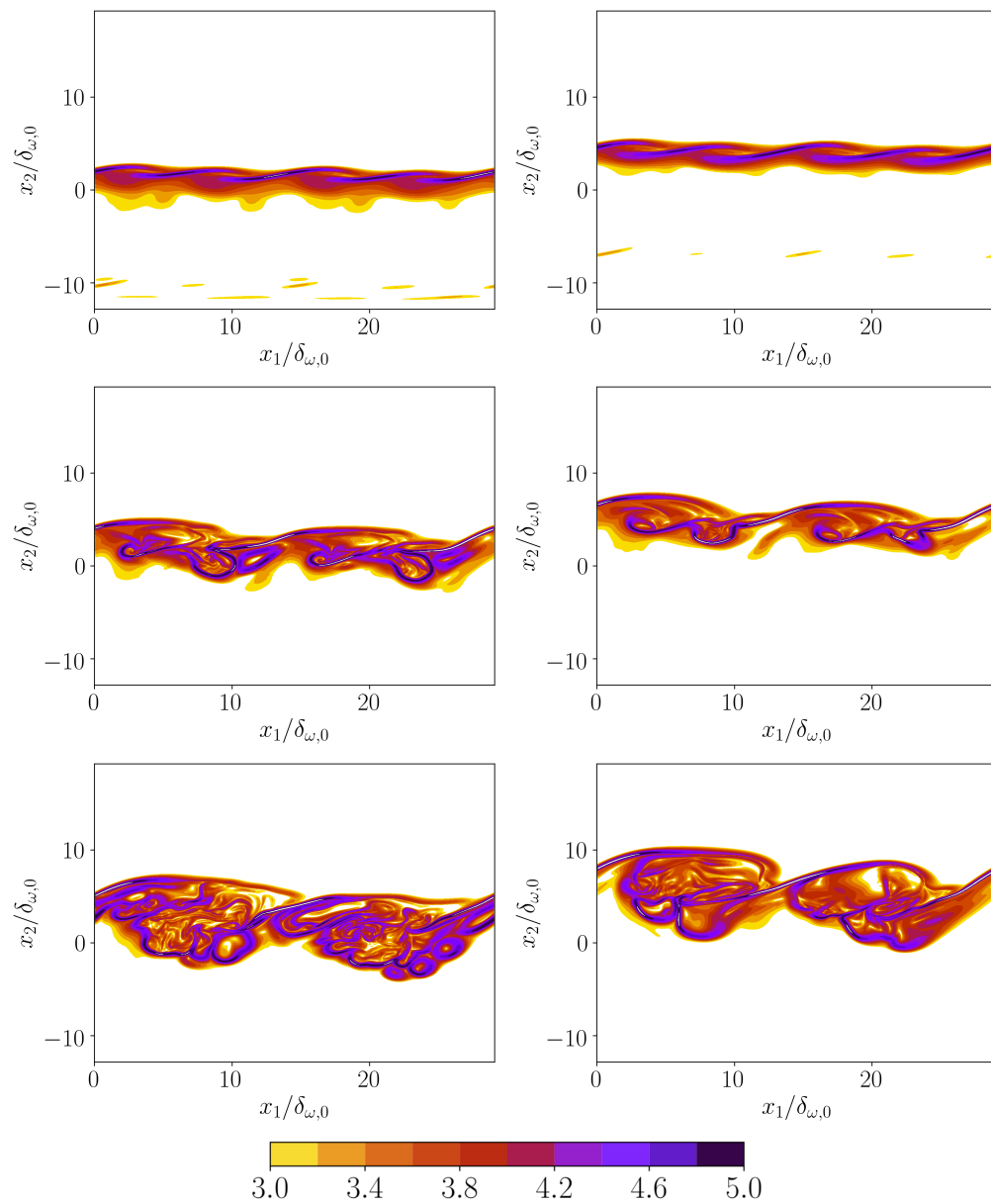


Fig. 6 Distribution in the $x_3/L_3 = 1/16$ plane of the density gradient in $\log_{10} |\nabla \rho|$ for (tab) - left column, and (gc) - right columns, for $t^* = [20, 40, 60]$ from top to bottom.

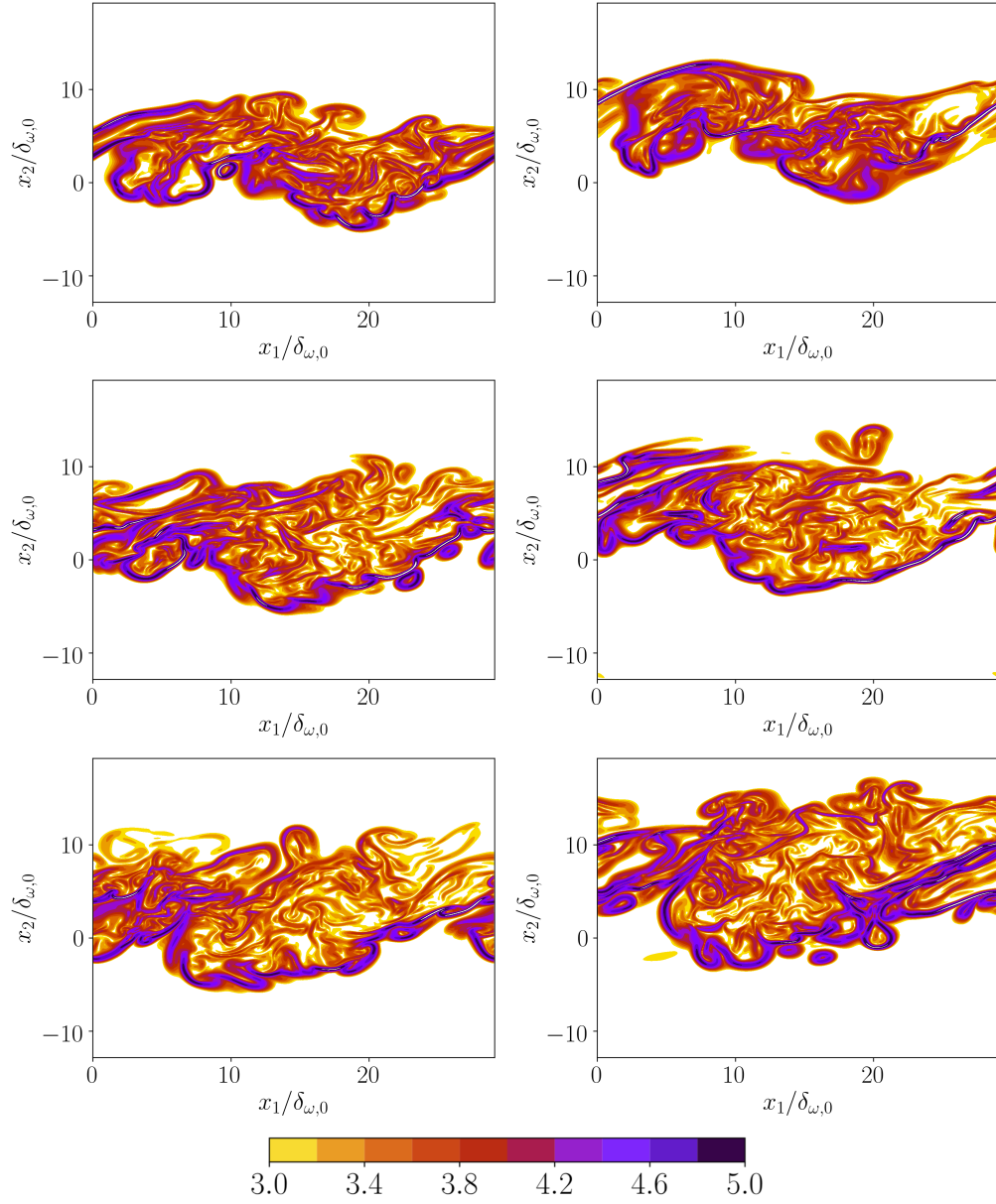


Fig. 7 Distribution in the $x_3/L_3 = 1/16$ plane of the density gradient in $\log_{10} |\nabla \rho|$ for (tab) - left column, and (gc) - right columns, for $t^* = [80, 100, 120]$ from top to bottom.

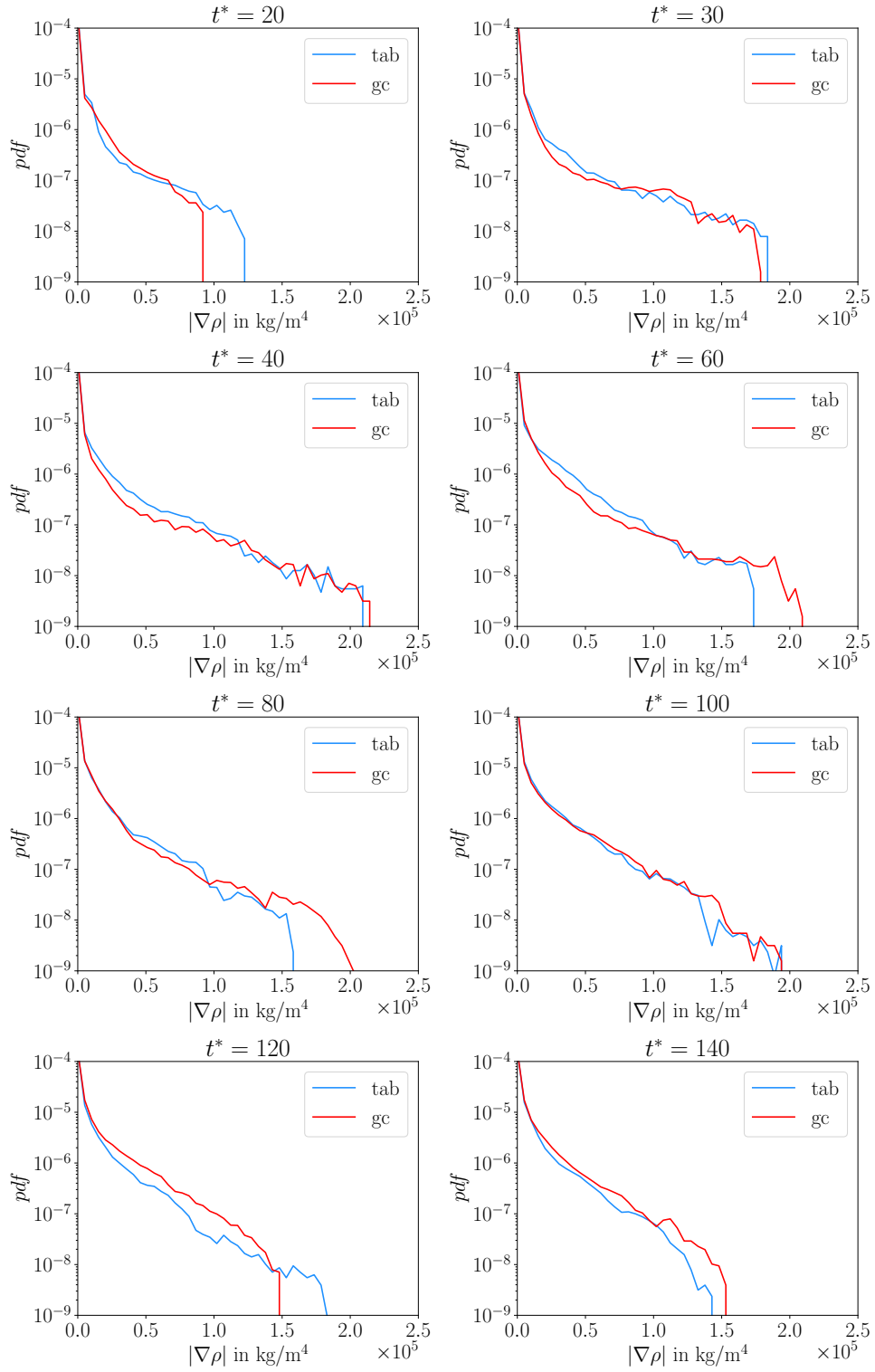


Fig. 8 Probability density distribution of the density gradient in the $x_3/L_3 = 1/16$ plane.

Acknowledgments

This study was sponsored at the California Institute of Technology by the Department of Energy, Basic Energy Science, with Dr. Wade Sisk as grant monitor. The authors would like to thank Dr. J.-N. Jaubert for providing the code to compute the group-contribution binary interaction coefficients. The computations were performed at the NAS NASA supercomputer facility, and we gratefully acknowledge the allocation from the T3 program directed by Dr. Michael M. Rogers.

References

- [1] Peng, D.-Y., and Robinson, D. B., "A new two-constant equation of state," *Ind. Eng. Chem. Res.*, Vol. 15, No. 1, 1976, pp. 59–64.
- [2] Prausnitz, J. M., Lichtenthaler, R. N., and de Azevedo, E. G., *Molecular Thermodynamics of Fluid-Phase Equilibria*, 2nd ed., Prentice-Hall, 1985.
- [3] Bellan, J., "Supercritical (and subcritical) fluid behavior and modeling: drops, streams and mixing layers, jets and sprays," *Progress in Energy and Combustion Science*, Vol. 26, 2000, pp. 329–366.
- [4] Oefelein, J. C., "Mixing and combustion of cryogenic oxygen-hydrogen shear-coaxial jet flames at supercritical pressure," *Combust. Sci. Technol.*, Vol. 178, 2006, pp. 229–252.
- [5] Reid, R. C., Prausnitz, J. M., and Poling, B. E., *The Properties of Gases and Liquids*, 4th ed., McGraw Hill, 1987.
- [6] Elliott, J., and Lira, C., *Introductory Chemical Engineering Thermodynamics*, Prentice Hall, 2012.
- [7] Knapp, H., Döring, R., Oellrich, L., Plöcker, U., and Prausnitz, J. M., "Vapor–liquid Equilibria for Mixtures of Low Boiling Substances," *Dechema*, Vol. VI, 1982.
- [8] Okong'o, N., and Bellan, J., "Direct numerical simulation of O₂/H₂ temporal mixing layers under supercritical conditions," *AIAA Journal*, Vol. 40, 2002, pp. 914–926.
- [9] Masi, E., Bellan, J., Harstad, K. G., and Okong'o, N. A., "Multi-species turbulent mixing under supercritical-pressure conditions: modelling, direct numerical simulation and analysis revealing species spinodal decomposition," *Journal of Fluid Mechanics*, Vol. 721, 2013, pp. 578–626.
- [10] Keizer, J., *Statistical Thermodynamics of Nonequilibrium Processes*, Springer Verlag, New York, 1987.
- [11] Harstad, K. G., and Bellan, J., "Mixing rules for multicomponent mixture mass diffusion coefficients and thermal diffusion factors," *Journal of Chemical Physics*, Vol. 120, No. 12, 2004, pp. 5664–5673.
- [12] Lee, B. I., and Kesler, M. G., "A Generalized Thermodynamic Correlation based on Three-Parameter Corresponding States," *AIChE Journal*, Vol. 21, No. 3, 1975, pp. 510–527.
- [13] Sciacovelli, L., and Bellan, J., "The influence of the chemical composition representation according to the number of species during mixing in high-pressure turbulent flows," *Journal of Fluid Mechanics*, Vol. 863, 2019, p. 293–340. doi: 10.1017/jfm.2018.992.
- [14] van Konynenburg, P. H., and Scott, R. L., "Critical lines and phase equilibria in binary van der Waals mixtures," *Philosophical Transactions of the Royal Society, London, Series A*, Vol. 298, No. 1442, 1980, pp. 495–540.
- [15] Jaubert, J.-N., and Mutelet, F., "VLE predictions with the Peng–Robinson equation of state and temperature dependent k_{ij} calculated through a group contribution method," *Fluid Phase Equilibria*, Vol. 224, 2004, pp. 285–304.
- [16] Jaubert, J.-N., Vitu, S., Mutelet, F., and Corriou, J.-P., "Extension of the PPR78 model (predictive 1978, PengRobinson EOS with temperature dependent k_{ij} calculated through a group contribution method) to systems containing aromatic compounds," *Fluid Phase Equilibria*, Vol. 237, 2005, pp. 193–211.
- [17] Privat, R., Jaubert, J.-N., and Mutelet, F., "Use of the PPR78 model to predict new equilibrium data of binary systems involving hydrocarbons and nitrogen. Comparison with other GCEOS," *Industrial Engineering Chemical Research*, Vol. 47, 2008, pp. 7483–7489.
- [18] Benson, S. W., and Buss, J. H. ., "Additivity rules for the estimation of molecular properties. Thermodynamic properties." *Journal of Chemical Physics*, Vol. 29, No. 3, 1958, pp. 546–572.

- [19] Kourdis, P. D., and Bellan, J., “Heavy-alkane oxidation kinetic-mechanism reduction using dominant dynamic variables, self similarity and chemistry tabulation,” *Combustion and Flame*, Vol. 161, 2014, pp. 1196–1223.
- [20] Xu, X., Privat, R., and Jaubert, J.-N., “Addition of the Sulfur Dioxide Group (SO₂), the Oxygen Group (O₂), and the Nitric Oxide Group (NO) to the E-PPR78 Model,” *Industrial & Engineering Chemistry Research*, Vol. 54, No. 38, 2015, pp. 9494–9504. doi:10.1021/acs.iecr.5b02639.